Received: 24 July 2019 | Revised: 30 March 2020 | Accepted: 7 April 2020

DOI: 10.1002/joc.6600

RESEARCH ARTICLE

International Journal of Climatology RMetS

Study on the differences in water vapour characteristics and predictive signals of low-frequency precipitation in the pre-flood season of South China between flood and drought years

Liping Li[1,2] | **Chenyu Ma**[1,2] | **Chunyan Yang**[3]

[1]Collaborative Innovation Center on Forest and Evaluation of Meteorological Disasters, NUIST, Nanjing, China

[2]Key Laboratory of Meteorological Disaster (NUIST), Ministry of Education, Nanjing, China

[3]Meteorological observatory, Qian Xinan Meteorologic Bureau, Guizhou, China

Correspondence
Liping Li, Collaborative Innovation Center on Forecast and Evaluation of Meteorological Disasters, Key Laboratory of Meteorological Disaster of Ministry of Education, College of Atmospheric Sciences, Nanjing University of Information Science and Technology, Nanjing 210044, China.
Email: li.liping@163.com

Funding information
National Key R&D Program of China, Grant/Award Number: 2018YFC1505602

Abstract

Using 753 station's precipitation daily data in China and NCEP/NCAR daily reanalysis data from 1980 to 2017, the lead–lag correlations between 10 and 20 days low-frequency (LF) precipitation and LF water vapour transport are comparatively analysed in the pre-flood season of South China during typical flood and drought years, and verified using Hybrid Single Particle Lagrangian Integrated Trajectory (HYSPLIT) backward trajectory model. The same features during both the flood and drought years include that, (a) the primary LF water vapour sources are the south side of Lake Baikal, the northern Sea of Japan and the Yellow Sea, the South China Sea and the western Pacific Ocean. (b)The key LF water vapour circulation systems are the Lake Baikal anticyclone (LBAC), the Northeast China cyclone (NECC), the Philippine Sea anticyclone (PSAC) and the South China cyclone (SCC). The different features between the flood and drought years include that, (a) the southern Sea of Japan is another water vapour source and the Australia anticyclone (AAC) is another key LF water vapour circulation system in the flood years. (b) There are two southwest warm water vapour flows and one southeast cross-equatorial water vapour flow in the flood years, while there is only one southwest warm water vapour flow in the drought years. In addition, most of notable predictive signals start appearing at approximately −4 days in both the flood and drought years. However, there is a difference in the time of occurrence of similar predictive signals, and some predictive signals only appear in the flood years.

KEYWORDS

low-frequency water vapour transport, predictive signals, pre-flood season of South China, the differences between flood and drought years

1 | INTRODUCTION

Low-frequency (LF) oscillations of the atmosphere include intraseasonal (30–60 days) and quasi-biweekly (10–20 days) oscillations (Li, 1993). Xie *et al.* (1963) mentioned the presence of a 40–50 days periodic oscillation in the Asian monsoon region. Later, Madden and Julian also found a 40–50 days LF oscillation in the tropical atmosphere and noted the prevalence of this type of intraseasonal oscillation across the globe (Madden and

Julian, 1971, 1972). Since then, research on atmospheric LF oscillations has gradually developed.

Atmospheric LF oscillations play a vital role in the formation and maintenance of persistent circulation anomalies (Ju *et al*., 2007) and are closely related to regional precipitation anomalies (e.g., Jones, 2000; Bond and Vecchi 2003; Barlow *et al*., 2005; Pohl *et al*., 2007; Jeong *et al*., 2008; Wheeler *et al*., 2009; Zhang *et al*., 2009). South China is situated in the East Asian monsoon region. Flood disasters in South China are closely related to atmospheric LF oscillations and their propagation (Tao and Wei, 2007). LF atmospheric signals from the subtropical and tropical regions produce LF convection and steady flows of water vapour from the oceans, which propagate in various directions to South China, resulting in the development and strengthening of LF convection over South China. For example, a persistent rainstorm event in South China in 1994 was closely related to the northward propagation of a 30–60 days tropical convection from the South China Sea (Shi and Ding 2000); a 10–20 days LF system at the 850-hPa level propagating from the tropical region was related to the LF precipitation during Guangdong's rainy season in 1999 (Tang *et al*., 2007); the northward propagation of an intraseasonal tropical monsoon (Lin *et al*., 2008) and the westward propagation of a 10–25 days LF tropical convection over the Western Pacific Ocean at approximately 150°E were related to persistent rainstorms in South China in mid-June 2005 (Bao, 2008). The time when the LF heat sources in the South China Sea propagate and the direction of the LF heat sources propagation over the tropical western Pacific Ocean are indicative of the total precipitation in South China in June (Gao *et al*., 2010). The positive-phase superposition of LF oscillations of various scales postponed the end of South China's pre-flood season in 2010 (Zhang *et al*., 2012). The impact of intraseasonal oscillations on the position and strength of a subtropical high results in changes of water vapour flux, thereby affecting LF precipitation in Guangdong in June (Lin *et al*., 2013). When the active center of Madden–Julian Oscillation (MJO) is located in the Indian Ocean(in the western Pacific Ocean), there is more(less) precipitation in South China (Zhang *et al*., 2011). This may be because the active (suppressed) MJO convection can stimulate Rossby waves that reach South China by diabatic heating, resulting in an anomalous ascending (descending) motion and a strengthening (weakening) of water vapour supply, thereby facilitating (inhibiting) precipitation in South China (Li *et al*., 2014a, 2014b).

Atmospheric LF oscillations from mid–high latitudes are also a cause of precipitation anomalies in South China. In the pre-flood season, LF wind fields at high and low latitudes simultaneously propagate toward South China, resulting in the extremely heavy precipitation (Xin *et al*., 2007). Precipitation in South China's pre-flood season in 2010 (Li *et al*., 2014b) and 2013 (Hu *et al*., 2014) was a result of the combined action of the transport of LF cold air from mid–high latitudes and LF water vapour from low latitudes. There were significant differences in the interaction, propagation characteristics and LF oscillation sources of upper- and lower-atmospheric LF circulations over mid–high and low latitudes between a typical flood year (2010) and a drought year (2004) (Xu *et al*., 2018). Before the occurrence of persistent heavy precipitation in May, the high-value region of LF diabatic heating propagates southward from north of 30°N (107–115°E) to South China (Hong *et al*., 2015). Water vapour (including cold air) affecting 10–20 days precipitation in South China's pre-flood season originates primarily from southwest, southeast, northeast and northwest of South China (Li *et al*., 2017). The superposition of a 10–20 days LF teleconnection wave train from Western Siberia at mid–high latitudes and LF signals from the tropical eastern Indian Ocean, together with LF water vapour transport, caused persistent LF precipitation anomalies in South China's pre-flood season in 2010 (Miao *et al*., 2017).

In summary, previous studies demonstrate that LF atmospheric circulation signals affecting LF precipitation in South China's pre-flood season originate from the tropical and subtropical regions, as well as mid–high latitude regions. However, the existing research is primarily focused on individual heavy-precipitation years, and the results, to an extent, lack universality. Thus, it is necessary to systematically compare the effects of LF oscillations on LF precipitation in multiple flood and drought years. Thus, this study comparatively examine the lead–lag correlations between LF water vapour circulation and LF precipitation in South China's pre-flood season for multiple flood and drought years, since 1980. It reveals the key water vapour circulation systems, the water vapour sources, and the meaningful predictive signals of LF precipitation during the flood and drought years, which can provide a valuable reference for extended range forecast of precipitation in South China.

2 | DATA AND METHODS

The data used in this study include (a) 2.5° × 2.5° global daily wind field and specific humidity reanalysis data, provided by the United States National Centers for Environmental Prediction/National Center for Atmospheric Research (NCEP/NCAR) (Kistler *et al*., 2001), (b) 2° × 2°

monthly Extended Reconstructed Sea Surface Temperature V5, provided by National Oceanic and Atmospheric Administration (NOAA) (Huang *et al*., 2017), (c) 2.5° × 2.5° NOAA data driving HYSPLIT mode (ftp://arlftp.arlhq.noaa.gov/pub/archives/reanalysis/RP.gbl), and (d) daily precipitation data recorded at 753 stations provided by the National Meteorological Information Center (China). The data are all for the period 1980–2017. South China is defined as the region 105–120°E, 20–27.5°N, within which there are 89 observation stations (Figure 1). The period April–June is defined as pre-flood season.

The Morlet wavelet analysis method (Wu and Wu, 2005) is used to analyse the prominent LF period of precipitation during the pre-flood season in South China, and a Butterworth Band-pass Filter (Murakami, 1984) is used to filter the prominent LF period. In addition, the relationship between LF precipitation and LF water vapour transport is analysed using the phase composite (Chan *et al*., 2002; Mao and Wu, 2005) and lead–lag correlation methods (Wei, 2009) (see Appendix A for details). HYSPLIT backward trajectory model is used to verify the results of lead–lag correlation (Draxler and Hess, 1998) (see Appendix B for details).

3 | COMPARISON OF THE LF CHARACTERISTICS OF PRECIPITATION DURING SOUTH CHINA'S PRE-FLOOD SEASON FOR FLOOD AND DROUGHT YEARS

Based on the normalized time series of the regional mean total precipitation at 89 stations during South China's pre-flood season for the period 1980–2017 (Figure 2) and a standard of ±1, eight (1993, 1998, 2001, 2005, 2006, 2008, 2010 and 2016) and seven (1985, 1988, 1991, 1995, 1999, 2004 and 2011) years are selected as typical flood and drought years, respectively. Accordingly, the precipitation characteristics (significant LF period, LF component intensity and variance contribution ratio) for the flood and drought years are compared.

3.1 | Comparison of significant LF precipitation periods in flood and drought years

In order to find the representative stations associated with LF precipitation, we look at the spatial deviation distributions of composite total precipitation after removing the domain means. Firstly, the composite total precipitation field for eight (seven) typical flood (drought) years in South China's pre-flood season is calculated by use of daily precipitation at 89 stations, and the spatial deviation field of composite total precipitation is obtained by removing the domain averages at each station for the typical flood (drought) years in South China's pre-flood season (Figure 3). Based on Figure 3, high-precipitation centers are found in northern Guangxi and central-northern Guangdong and at the junction of Fujian and Jiangxi during the flood years, with precipitation in Guangdong being the largest. This is in agreement with the findings of Li *et al*. (2017). The locations of the high-precipitation centers during the drought years are near those in the flood years. However, during the drought years, there are two precipitation centers in Guangdong and a high-precipitation center is also present at the northern junction of Hunan and Jiangxi. In addition, the maximum values at the precipitation centers are similar during the drought years. As shown in Figure 3, 20 (deviation values ≥ 200 mm) and 21 (deviation values ≥ 60 mm) stations are selected as representative stations for the flood and drought years, respectively, to further compare the significant LF characteristics of precipitation during the flood and drought years.

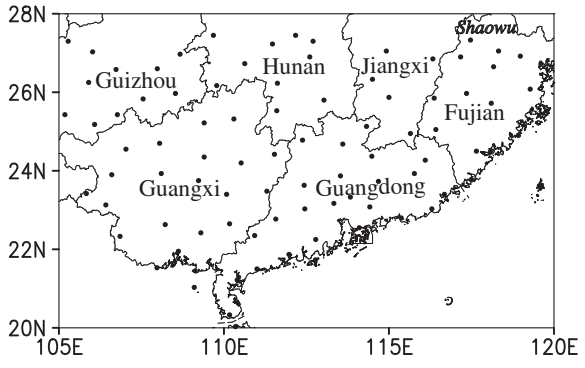

FIGURE 1 Eighty-nine observation stations in South China

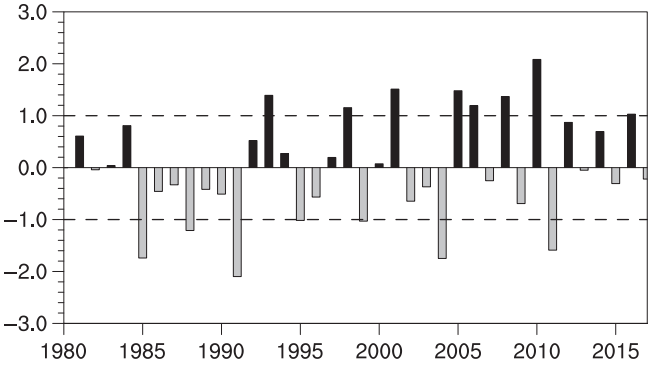

FIGURE 2 The normalized time series of the regional mean total precipitation during South China's pre-flood season for the period 1980–2017

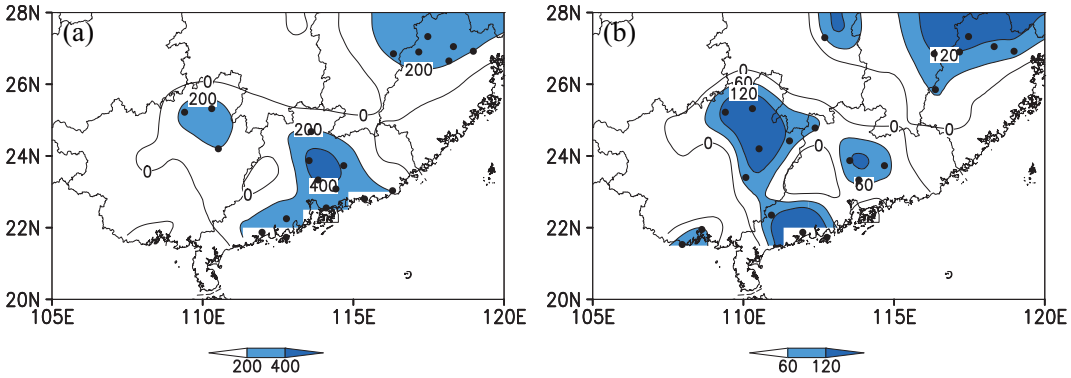

FIGURE 3 The spatial deviation fields of composite total precipitation after removing the domain means in South China's pre-flood season for the typical (a) flood and (b) drought years. The black dots indicate the stations where deviation values ≥200(60) mm in flood (drought) years (mm) [Colour figure can be viewed at wileyonlinelibrary.com]

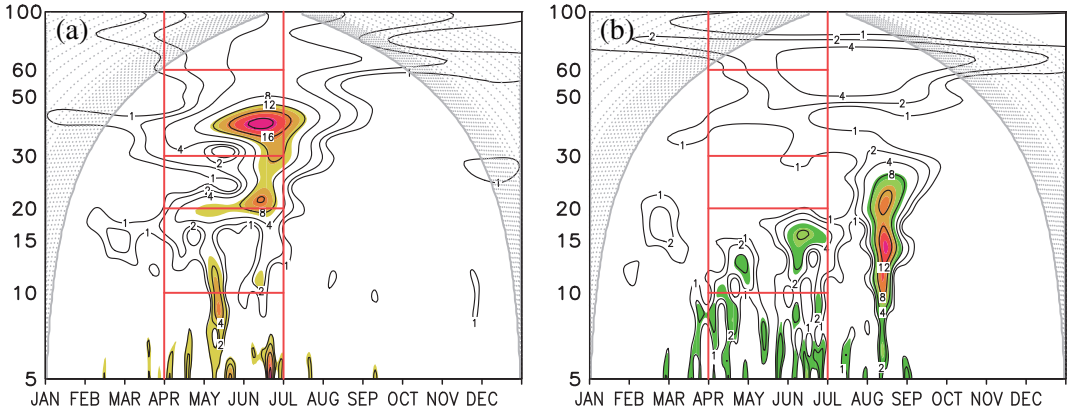

FIGURE 4 The wavelet analysis results for the mean daily precipitation series at Shaowu station in Fujian in South China's pre-flood season for the typical (a) flood and (b) drought years (shading are significant at $\alpha = .05$ level) [Colour figure can be viewed at wileyonlinelibrary.com]

The wavelet analysis results of mean daily precipitation series at Shaowu station in Fujian for the typical flood and drought years (Figure 4), which is located in one of the high-precipitation centers, are used as an illustrative example. As indicated in Figure 4, 10–15 days and 20–50 days periods are significant during the flood years and 10–20 days is significant during the drought years. The significant LF periods of mean daily precipitation series at each representative station during South China's pre-flood season in the flood (Figure 5a) and drought (Figure 5b) years are further provided. As indicated in Figure 5, the 10–20 days, 20–30 days and 30–60 days significant periods of precipitation are present at 19 (21), 10 (5) and 11 (3) representative stations in the flood (drought) years. Evidently, 10–20 days period is the most significant in the flood and drought years. However, the stations with significant 20–30 days and 30–60 days periods in the flood years are more than in the drought years.

3.2 | Comparison of intensity and variance contribution ratio of LF precipitation between flood years and drought years

The LF oscillation intensity of precipitation is represented by the standard deviation of its LF filtering sequence (Figure 6), and the greater the standard deviation, the stronger the oscillation is. Variance contribution ratio (figure not shown) is the percentage of the variance of each LF component to the variance of the 10–90 days LF component. As shown in Figure 6, the strong oscillation areas of each LF component in the flood and drought years approximately correspond to the high-precipitation areas (Figure 3). The 10–20 days component is the strongest, followed by the 30–60 days and 20–30 days components. Moreover, the oscillation intensity of each LF component is higher in the flood years than in the drought years. No definite relationship is found between

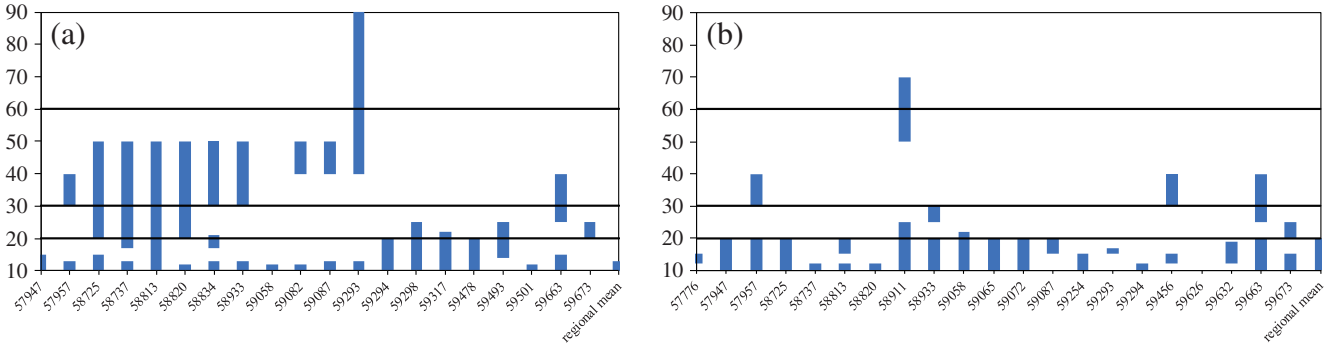

FIGURE 5 The significant LF oscillation periods of mean daily precipitation series at each representative station during South China's pre-flood season for the typical (a) flood and (b) drought years (unit: D), horizontal coordinates are station number [Colour figure can be viewed at wileyonlinelibrary.com]

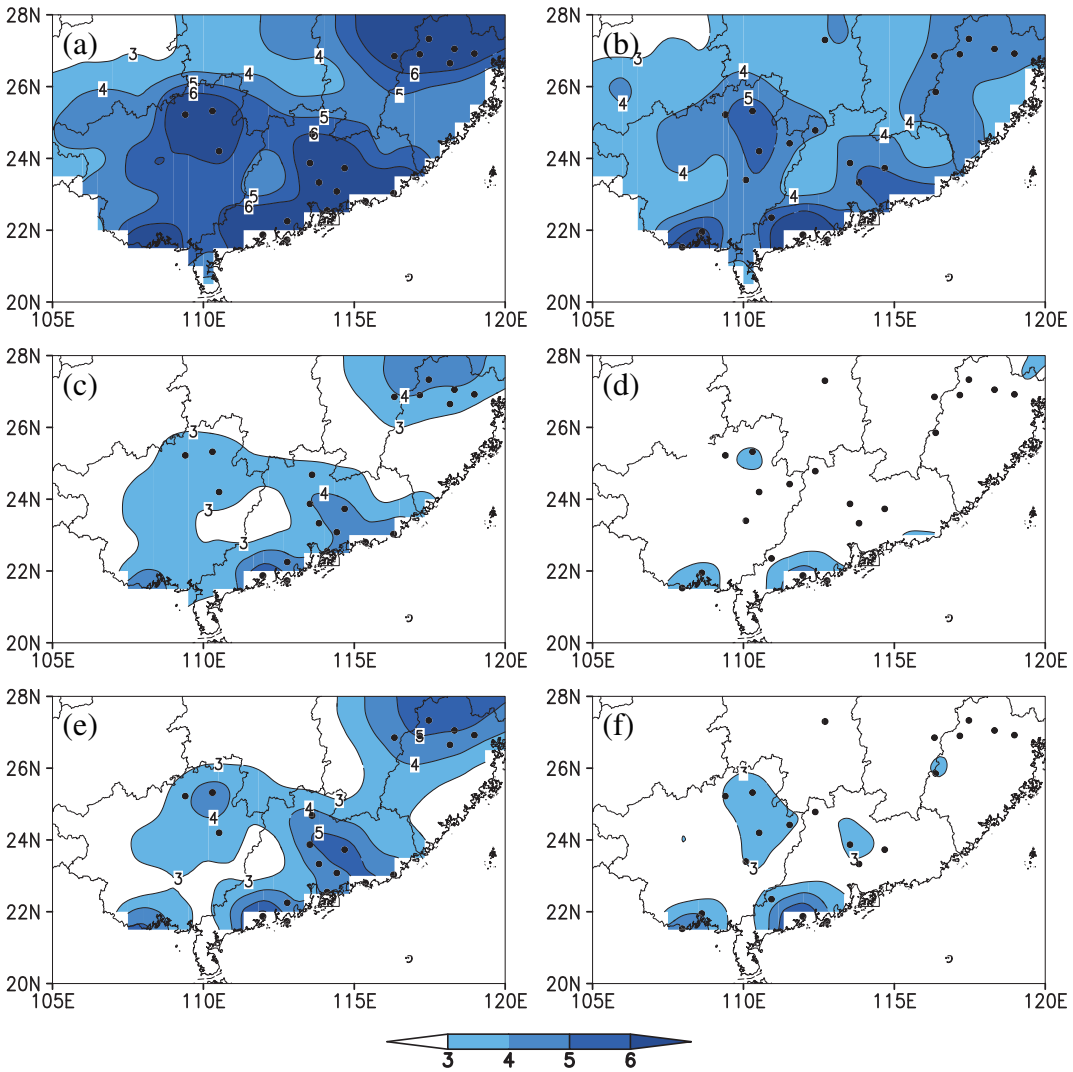

FIGURE 6 The standard deviation fields of the 10–20 days (a, b), 20–30 days (c, d) and 30–60 days (e, f) significant LF components of precipitation during the flood (a, c, e) and drought (b, d, f) years (mm) [Colour figure can be viewed at wileyonlinelibrary.com]

the high-variance contribution ratio areas and the high-precipitation areas. The 10–20 days, 20–30 days and 30–60 days components account for approximately 50–60%, 15–20% and 20–25%, respectively, and there is no significant difference between the flood and drought years (figure not shown).

In summary, in the flood and drought years, the 10–20 days LF component is the most important, with a variance contribution ratio of over 50%. Thus, in the following sections, only the LF water vapour fields related to the 10–20 days LF precipitation during flood and drought years are comparatively analysed.

4 | COMPARISON OF THE CHARACTERISTICS OF LF WATER VAPOUR CIRCULATIONS AFFECTING LF PRECIPITATION DURING FLOOD AND DROUGHT YEARS

The characteristics of LF water vapour circulations related to LF precipitation are examined using the phase composite method. One standard deviation of the 10–20 days filter precipitation series is selected as the threshold. Complete fluctuations with amplitude greater than the threshold are selected. Subsequently, each fluctuation is divided into eight phases. Phase 1 (5) represents the transition of the oscillation from the dry phase (wet phase) to the wet phase (dry phase); phase 3 (7) corresponds to the peak (valley) of wet phase (dry phase); and phases 2 and 4 (6 and 8) correspond to the half of the peak (valley) values (figure not shown). The 10–20 days column-integrated LF water vapour fluxes and the corresponding water vapour flux divergence during the flood and drought years are composited based on the eight phases mentioned above, respectively. The analysis focus on the characteristics at the peak phase 3 during the flood (Figure 7a) and drought (Figure 7b) years. For simplicity, the cyclone (anticyclone) below represents LF cyclonic (anticyclonic) water vapour circulation, and the water vapour flow is written as WVF for short. Similarly,

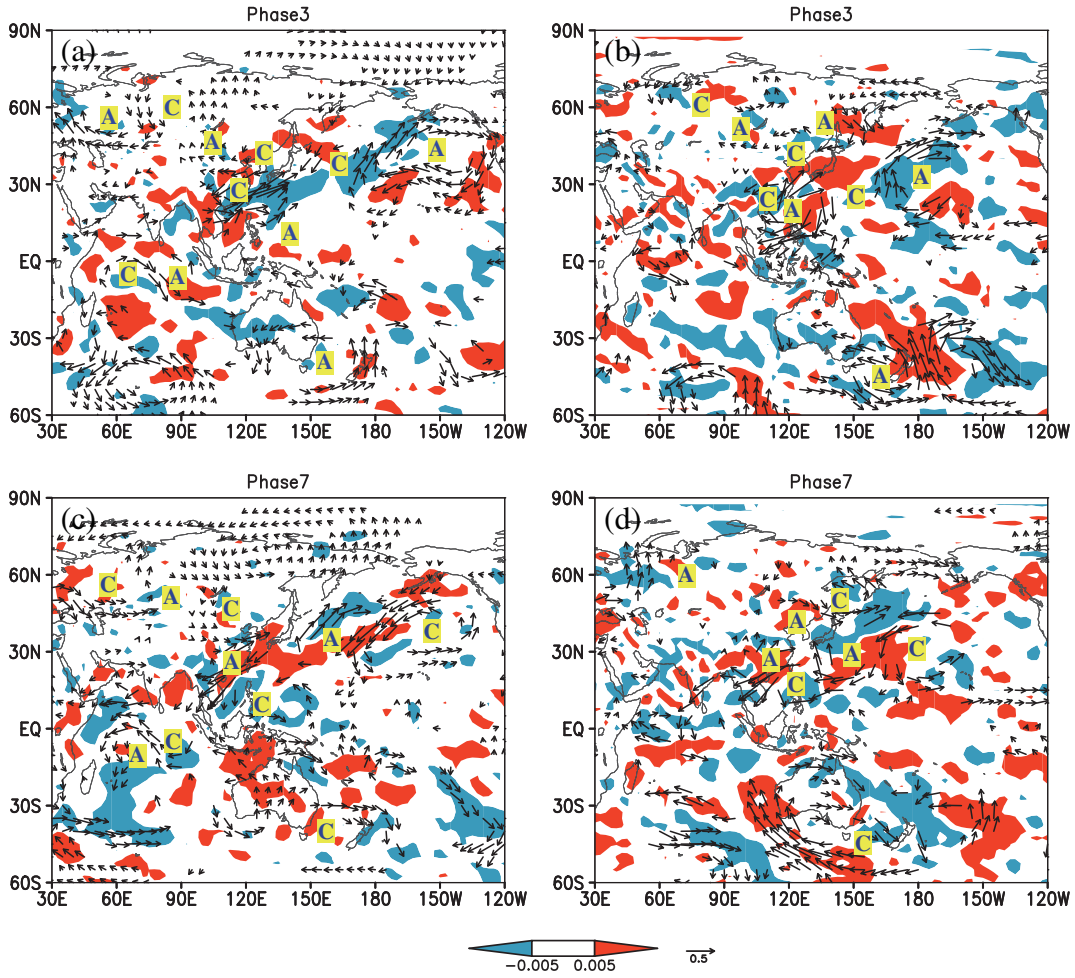

FIGURE 7 Composite of the 10–20 days column-integrated water vapour flux (vector, 105 $g^{-1}{\cdot}s^{-1}$, significant at $\alpha = .1$ level) and the corresponding water vapour flux divergence fields (shaded, $gm^{-2}{\cdot}s^{-1}$) based on the peak phase 3 (a, b) and the valley phase 7 (c, d) of 10–20 days LF precipitation during the flood (a, c) and drought (b, d) years. A and C represent anticyclonic and cyclonic water vapour circulation, respectively [Colour figure can be viewed at wileyonlinelibrary.com]

the cross-equatorial water vapour flow is called CEWVF for short.

As can be seen from Figure 7, (1) the cold water vapour wave trains in the northwest and the northerly directions are different in the flood and drought years. An anticyclone is present over the Ural Mountains during the flood years but absent during the drought years. Lake Baikal and Northeast China is controlled by an anticyclone and a cyclone in the flood years, respectively; the anticyclone near Lake Baikal expands eastward to the Sea of Okhotsk and the cyclone over Northeast China is relatively weak in the drought years. As a result, there is more dry-cold air from the south side of Lake Baikal, but less wet-cold water vapour from the northern Sea of Japan in the flood years than in the drought years.

(2) In the northeast direction, the range and intensity of the water vapour wave train differs in the flood and drought years. There is an anticyclonic–cyclonic–anticyclonic wave train extending from the northeastern Pacific Ocean to the Philippine Sea. It is worth noting that the LF water vapour circulations in the northeastern wave train cover wider meridional range and are stronger in the flood years than in the drought years, and consequently the anticyclone over the Philippine Sea is able to transport more wet-warm water vapour from the South China Sea and the western Pacific Ocean to South China in the flood years.

(3) Wet-warm WVFs in the southwest and southeast directions are different in the flood and drought years. During the flood years, there are two wet-warm WVFs in the southwest direction and one CEWVF in the southeast direction. Specifically, in the southwest direction, one (relatively weak) extends from the Arabian Sea to the Bay of Bengal, the other cross-equatorially connected by a pair of vortices over the equatorial Indian Ocean extends from Somalia to the equatorial Indian Ocean to Sumatra. They merge over the Indochina peninsula and then transport water vapour to South China. In the southeast direction, the wet-warm CEWVF connected by two anticyclones, one over Australia and the other over the Philippine Sea, extends from New Guinea to Kalimantan to the South China Sea. During the drought years, there is only one wet-warm CEWVF in the southwest direction extending from the Arabian Sea (relatively weak) and the Maldives to the Indian peninsula to the Bay of Bengal to the Indochina peninsula to South China.

(4) The movement of wave trains are different in the flood and drought years. From phase 1 to phase 3 (figures for phase 1 and phase 2 not shown), the LF water vapour wave trains or circulation systems in the Southern and Northern Hemispheres significantly move and strengthen to South China in the flood years. Whereas the movement is inconspicuous and, overall, the strength of the systems undergoes changes in the drought years,.

(5) The cyclone controlling South China also merges the wet-cold water vapour from the Yellow Sea (and the southern Sea of Japan in the flood years) with the cold and wet-warm WVFs mentioned above, resulting in the heavy LF precipitation in South China.

In summary, there are four similar LF key water vapour circulation systems in the flood and drought years, including the Lake Baikal anticyclone (LBAC) bringing dry-cold air from the south side of Lake Baikal, the Northeast China cyclone (NECC) bring wet-cold WVF from the northern Sea of Japan, the Philippine Sea anticyclone (PSAC) bringing wet-warm WVF from the South China Sea and the western Pacific Ocean, the South China cyclone (SCC) bringing wet-cold WVF from the Yellow Sea (and the southern Sea of Japan in the flood years) and wet-warm WVFs in the southwest direction. In addition, there is the Australia anticyclone (AAC) in the flood years forming CEWVF in the southeast direction.

During the flood and drought years, the characteristics of LF water vapour circulations at the phase 7 (Figure 7c,d) are essentially opposite to the phase 3 (Figure 7a,b). South China is controlled by an anticyclone and divergent water vapour conditions. LF precipitation is interrupted at the phase 7.

5 | LEAD–LAG CORRELATION BETWEEN LF PRECIPITATION AND WATER VAPOUR DURING THE FLOOD AND DROUGHT YEARS AND PREDICTIVE SIGNALS OF LF PRECIPITATION

5.1 | Lead–lag correlation analysis

In order to understand the characteristics of LF water vapour circulation in the early stage and find predictive signals of LF precipitation, the vector fields composed of lead–lag correlation coefficients between column-integrated LF meridional and latitudinal water vapour fluxes 8–0 days in advance and LF precipitation are analysed for the flood (Figure 8) and drought (Figure 9) years, with the time intervals 2 days (see Appendix A for calculation ideas). The vector direction reflects the transport direction of the correlated LF water vapour flux. The magnitude of the vector module reflects the degree of correlation. The red trajectories in Figures 8 and 9 indicate of wet-warm WVFs for the sake of clarity.

5.1.1 | Flood years

As demonstrated in Figure 8, the correlated LF water vapour circulations at −8 to −6 days exhibit similar characteristics. To be specific, in the northwest direction, there is an anticyclone over Western Siberia and a cyclone over Northeast China (NECC). In the northeast direction, there is a cyclonic–anticyclonic–cyclonic wave train extending from the northeastern Pacific Ocean to the Philippine Sea. In the southern direction, there is an anticyclonic–cyclonic vortex pair over the southeastern Indian Ocean and southern Australia. South China is controlled by an anticyclone and LF divergent water vapour conditions. At −6 days, the northeastern wave

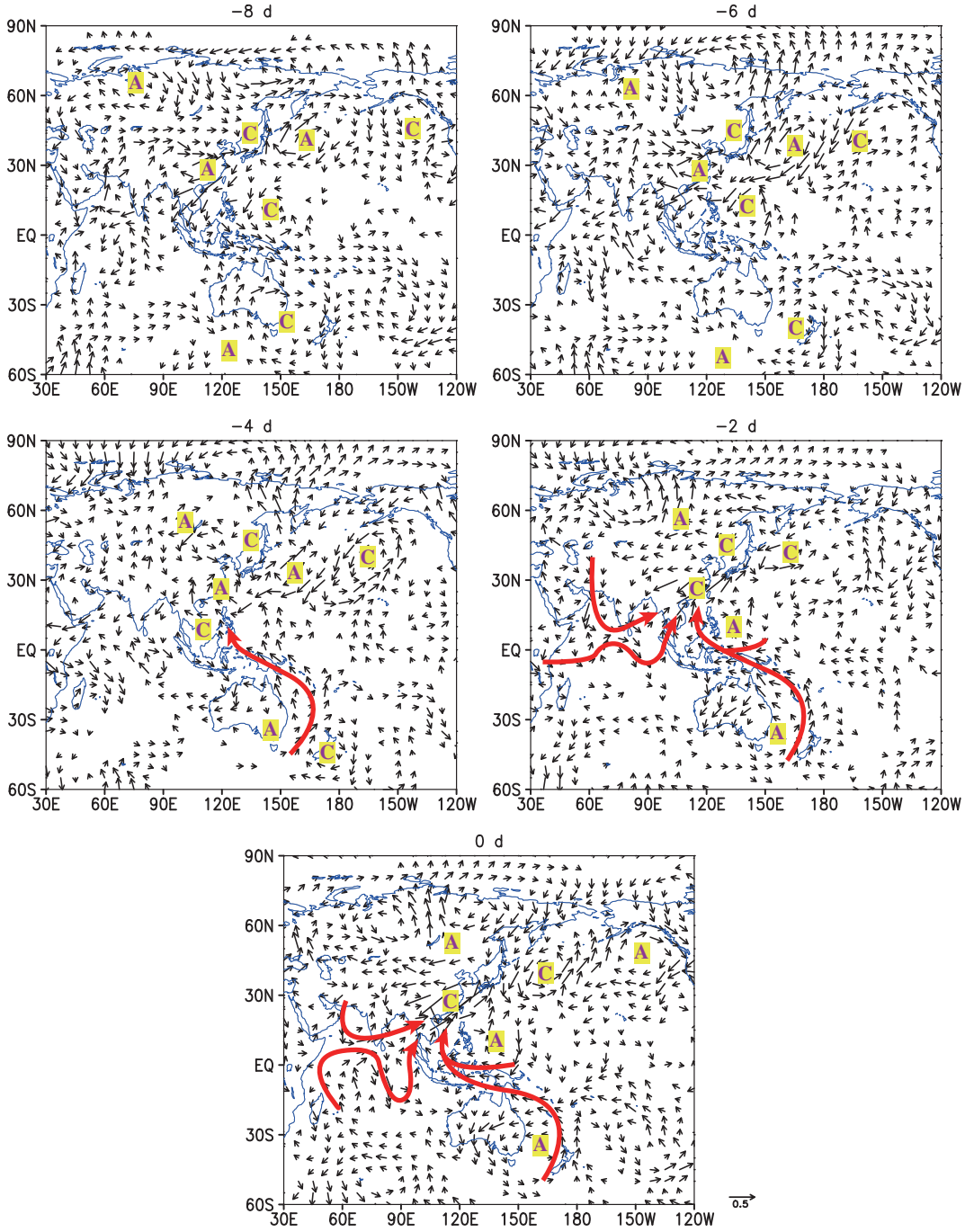

FIGURE 8 The vector fields composed of lead–lag correlation coefficients between column-integrated LF meridional and latitudinal water vapour fluxes 8–0 days ahead and LF precipitation for the flood years, with time intervals of 2 days (significant at $\alpha = .05$ level). A and C represent anticyclonic and cyclonic LF water vapour circulation systems, respectively, and the long red trajectories are drawn as a schematic diagrams of wet-warm water vapour channels [Colour figure can be viewed at wileyonlinelibrary.com]

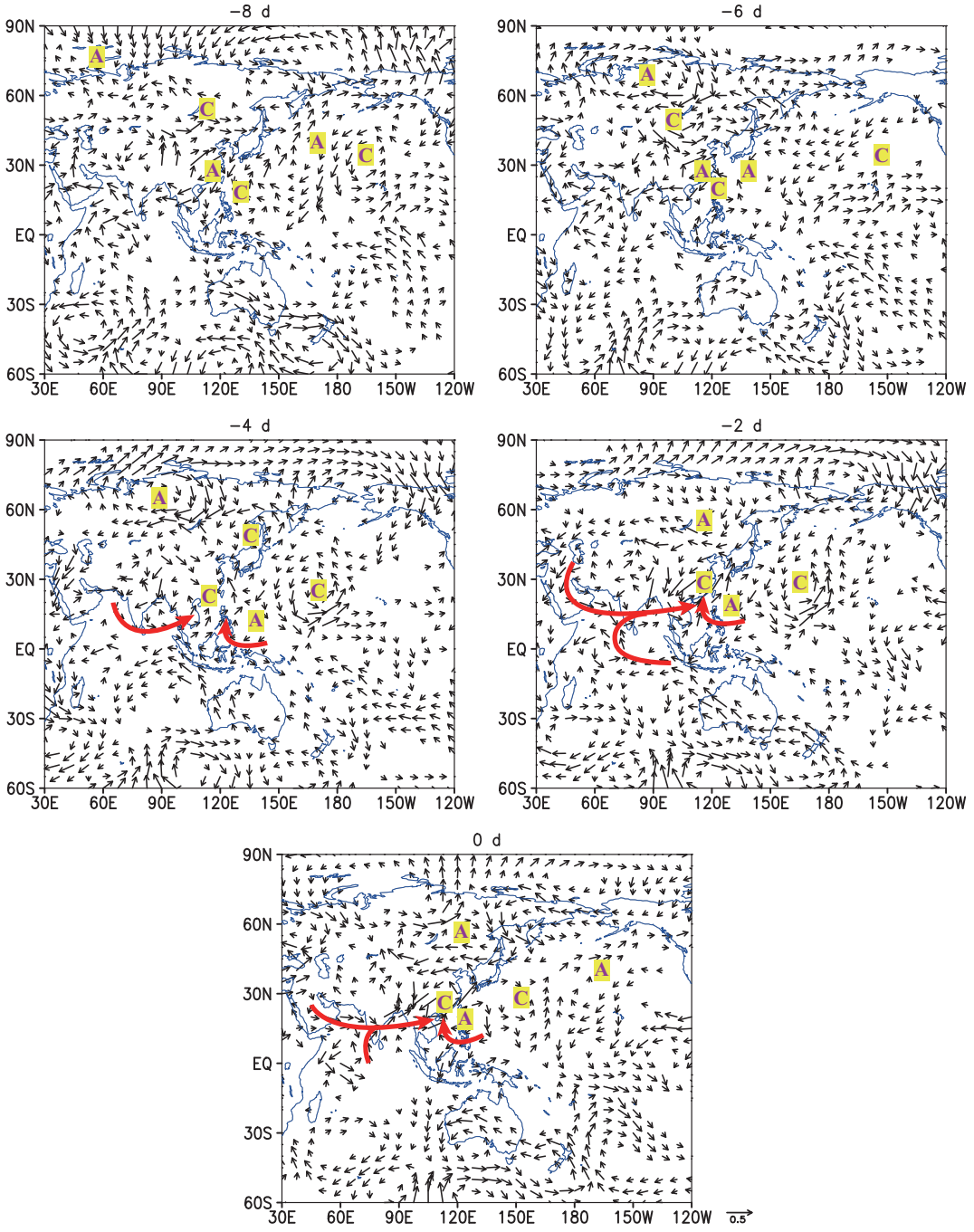

FIGURE 9 The vector fields composed of lead–lag correlation coefficients between column-integrated LF meridional and latitudinal water vapour fluxes 8–0 days ahead and LF precipitation for the drought years, with time intervals of 2 days (significant at $\alpha = .05$ level). A and C represent anticyclonic and cyclonic LF water vapour circulation systems, respectively, and the long red trajectories are drawn as a schematic diagrams of wet-warm water vapour channels [Colour figure can be viewed at wileyonlinelibrary.com]

train moves toward South China. South China anticyclone and Northwest Pacific anticyclone approaches gradually.

At −4 days, in the northwest direction, the anticyclone moves to Lake Baikal, namely Lake Baikal anticyclone (LBAC). In the northeast direction, the wave train continuously moves toward South China. In the southeast direction, the previous anticyclone over the southeastern Indian Ocean moves northeastward to southern Australia, which is called Australia anticyclone (AAC), thereby resulting in the formation of a CEWVF extending from the southwestern Pacific Ocean to New Guinea to the Philippine archipelago to the South China Sea. The Philippine Sea cyclone continuously moves

toward South China Sea. South China anticyclone moves eastward into the sea, approaching further to Northwest Pacific anticyclone.

At −2 days, both LBAC and NECC strengthen in the northwest direction. South China anticyclone and Northwest Pacific anticyclone merge and form the Philippine Sea anticyclone (PSAC). The PSAC and enhanced AAC further strengthen the southeast CEWVF. In the southwest direction, two wet-warm WVFs reach South China after merging in the Indochina Peninsula, one extending from east of the Caspian Sea to the Arabian Sea to the Bay of Bengal, and the other extending from Somalia to the equatorial Indian Ocean to Sumatra. Under the interaction of two southwest WVFs and one southeast CEWVF, the previous Philippine Sea cyclone moves northward into South China and form South China cyclone (SCC). A LF water vapour environment favourable to heavy precipitation in South China is basically formed.

At 0 days, the eastward expansion of LBAC allows the NECC to move southward and incorporate into SCC, further strengthening SCC. Both PSAC and AAC further intensify, resulting in the strengthening of the southeast CEWVF. The southeast CEWVF moves westward to Kalimantan from the Philippine archipelago. The two southwest WVFs are further strengthened, transporting more wet-warm water vapour from the Arabian Sea, the Bay of Bengal and the equatorial Indian Ocean to South China. The SCC merges the cold and wet-warm water vapour, resulting in the occurrence of LF heavy precipitation.

5.1.2 | Drought years

As shown in Figure 9, at −8 days, in the northwest direction, the region extending from Novaya Zemlya to Lake Baikal to South China is controlled by a significantly correlated LF anticyclonic–cyclonic–anticyclonic wave train. In the northeast direction, the region extending from the northeastern Pacific Ocean to the Philippine Sea is controlled by a significantly correlated LF cyclonic–anticyclonic–cyclonic wave train. At −6 days, the above two water vapour wave trains move further to South China, and South China anticyclone and Northwest Pacific anticyclone approaches more quickly in the drought years than in the flood years.

At −4 days, the significantly correlated wave trains in the northwest and northeast directions rapidly continue moving to South China. In the northwest direction, the cyclone moves from Lake Baikal to Northeast China, forming Northeast China cyclone (NECC). South China anticyclone and Northwest Pacific anticyclone merge southward and form the Philippine Sea anticyclone (PSAC). Meanwhile, the previous Philippine Sea cyclone moves northwest to South China, forming South China cyclone (SCC). The above three circulation systems are formed 2 days earlier in the drought years than in the flood years. In the southwest direction, the wet-warm WVF also appears 2 days earlier in the drought years than in the flood years, extending from the Arabian Sea to the Bay of Bengal to the Indochina peninsula to the South China Sea.

At −2 days, the anticyclone over the northwest side of Lake Baikal moves east of Lake Baikal, which is Lake Baikal anticyclone (LBAC). Meanwhile, the NECC moves southward and merges into the SCC. The PSAC intensifies and moves northward. The southwest wet-warm WVF is further strengthened, extending from the Caspian Sea and the equatorial central-eastern Indian Ocean near the Maldives to the South China. A LF water vapour environment favourable to heavy precipitation in South China is basically formed.

At 0 days, both LBAC and SCC further intensifies, and PSAC is closer to South China. The southwest WVF weakens slightly extending from the Arabian Sea and the Maldives to the Indian peninsula to the Bay of Bengal to the Indochina peninsula to South China. SCC combines cold and wet-warm water vapour, resulting in the occurrence of LF heavy precipitation in South China.

5.2 | Predictive signals

Clearly, during both the flood and drought years, starting from −8 days, attention should be given to whether some key water vapour circulation systems located in the northwest and northeast of South China move toward South China. In addition, except NECC appearing at −8 days in the flood years, all other notable predictive signals appear at approximately −4 days. According to the analysis in Section 5.1, Table 1 summarizes the development and movement of the key LF circulation systems and the corresponding wet-warm WVFs from −8 to 0 days in the flood and drought years. The key LF circulation systems in Table 1 are divided into four groups from north to south, including NECC, LBAC, SCC-PSAC and AAC.

5.3 | Verification of LF water vapour source and transport path based on HYSPLIT model

HYSPLIT model is an integrated model system for particle trajectory, diffusion and settlement analysis. It is developed by Air Resources Laboratory (ARL) of National Oceanic and Atmospheric Administration (NOAA) of the

TABLE 1 The key LF circulation systems and wet-warm WVFs as the predictive signals in the flood and drought years

	−8 to −6 days	−4 days	−2 days	0 days
NECC				
Flood	Appearing	Intensifying	Intensifying and moving southward	Merging with SCC
Drought	No	Appearing	Moving southward and merging with SCC	No
LBAC				
Flood	No	Appearing	Intensifying	Expanding eastward
Drought	No	No	Appearing	Intensifying
SCC-PSAC (southeast and southwest WVFs)				
Flood	No	No	Appearing (appearing)	Intensifying (intensifying)
Drought	No	Appearing (appearing)	Intensifying (intensifying)	Intensifying (maintaining)
AAC (southeast CEWVF)				
Flood	No	Appearing (appearing)	Intensifying (intensifying)	Intensifying (intensifying)
Drought	No	No	No	No

United States (Draxler and Hess, 1998). The model is divided into forward trajectory model and backward trajectory model, which is briefly described in Appendix B.

In this section, we will study the sources and transport paths of the water vapour for flood and drought years in the pre-flood season of South China using HYSPLIT backward trajectory model, respectively. The simulation objects are the three representative stations where the significant abnormal precipitation centers mentioned in Section 3.1 are located, namely, the Fogang station (113.53°E, 23.87°N) in Guangdong, Guilin station (110.3°E, 25.32°N) in Guangxi and Shaowu station (117.47°E, 27.33°N) in Fujian. For each station, there are $8 \times 91 = 728$ ($7 \times 91 = 637$) initial dates of simulation for eight (seven) typical flood (drought) years from April 1 to June 30, and the selected time step is 12 hr, that is, the track point positions at 0:00 and 12:00 are taken, and 1,500 m is selected as the simulation height, and the three-dimensional motion trails of the tracking 8 days backward of the gas block are simulated. The three-dimensional motion trails simulated are clustered, and the water vapour sources, the transport paths and the contribution rate are obtained for the three stations respectively (Figure 10).

Comparing the water vapour transport paths for flood (drought) years obtained in Section 5.1(Figures 8 and 9) with the results using HYSPLIT model for Fogang, Guilin and Shaowu stations (Figure 10), it can be seen that the HYSPLIT backward trajectory pattern can better verify the water vapour transport channels. For example, the warm WVFs in the southwest and southeast direction are more distinct for flood years in Figure 8, and the corresponding simulated channels in Figure 10 are also clearer. The southwest warm WVFs are clearer and southeast one is weaker without southeast CEWVF for drought years in Figure 9, and the simulated southwest water vapour channels are more distinct for three stations and the simulated southeast one only appear for Fogang station in Figure 10. The simulated northwest and northeast cold water vapour transport channels for flood and drought year in Figure 10 are both clear and similar to the results of Section 5.1.

6 | CONCLUSIONS AND DISCUSSION

6.1 | Conclusions

This study comparatively analysed the characteristics of LF precipitation and the lead–lag correlations between it and LF water vapour transport in the pre-flood season of South China during multiple typical flood and drought years, and determined the primary LF water vapour circulation systems (wave trains) affecting the LF precipitation, the LF water vapour sources and the predictive signals of LF precipitation during the flood and drought years. HYSPLIT model is also used to verify the results of lead–lag correlations. The main conclusions drawn are as follows:

1 In the pre-flood season of South China, during the flood and drought years, 10–20 days are the most significant LF periods of precipitation, followed by 30–60 days LF periods. The intensity of each LF component is higher during the flood years than during the drought years, but there is no significant difference in variance contribution ratio between the flood and drought years.

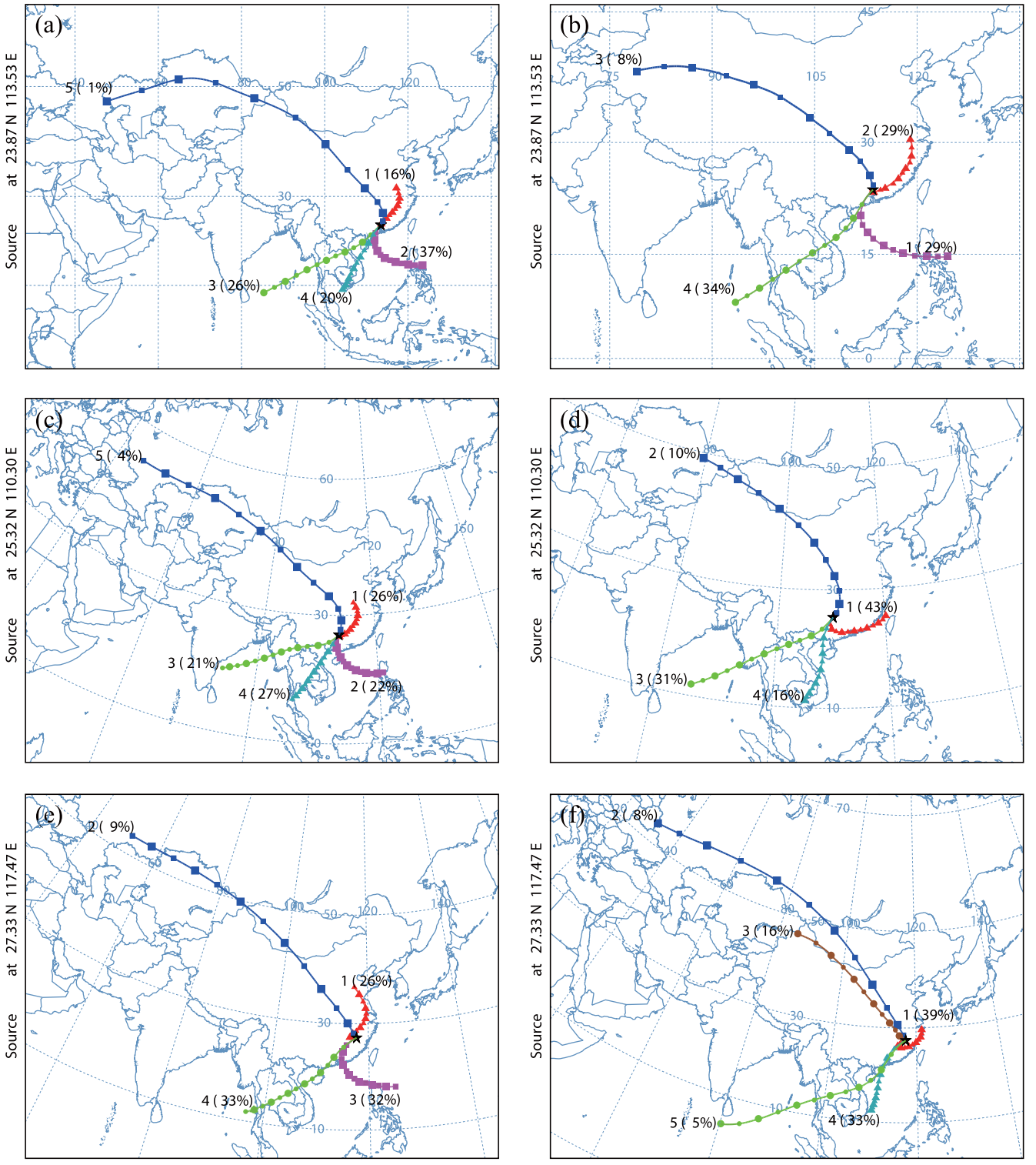

FIGURE 10 The simulated backward 8 days water vapour trajectories by HYSPLIT model for typical flood (a, c, e) and drought (b, d, f) years at Fogang (a, b), Guilin (c, d) and Shaowu (e, f) station in pre-flood season of South China. The percentage is the water vapour contribution ratio of the trajectory. The numbers from 1 to 5 represent the first to fifth water vapour channels [Colour figure can be viewed at wileyonlinelibrary.com]

2 During the flood and drought years, the key LF water vapour circulation systems and water vapour sources primarily include the Lake Baikal anticyclone (LBAC) bringing dry-cold air (more in the flood years) from the south side of Lake Baikal, the Northeast China cyclone (NECC) bringing wet-cold WVF (more in the

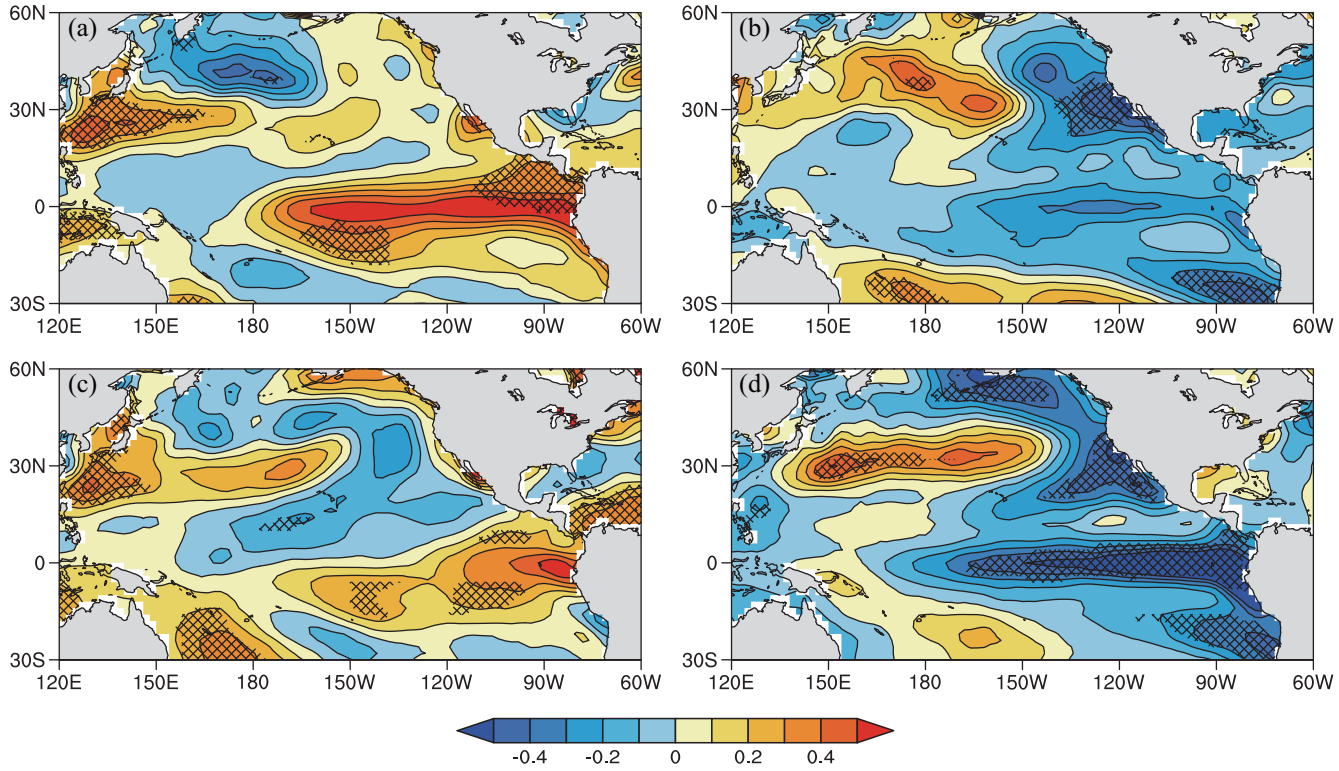

FIGURE 11 Composite of SST anomaly in the pre-winter (a, b) and pre-flood period (c, d) over the Pacific for the flood (a, c) and drought (b, d) years, respectively (× are significant at $\alpha = .05$ level, °C) [Colour figure can be viewed at wileyonlinelibrary.com]

drought years) from the northern Sea of Japan, the Philippine Sea anticyclone (PSAC) bringing wet-warm WVF from the South China Sea and the western Pacific Ocean and the South China cyclone (SCC) bringing wet-cold WVF from the Yellow Sea (and the southern Sea of Japan in the flood years) and the southwest wet-warm WVFs. In addition, the Australia anticyclone (AAC) in the flood years is also the key LF water vapour circulation system, which forms the southeast CEWVF originating from the southwestern Pacific Ocean. It is worth noting that the southwest wet-warm WVFs are different between the flood and drought years. During the flood years, there are two wet-warm WVFs in the southwest directions, and the WVFs originating from the Arabian Sea and the Bay of Bengal is relatively weak and the CEWVF originating from Somalia is relatively strong. While in the drought years, there is only one wet-warm CEWVF in the southwest direction originating from the Arabian Sea, the Maldives and the Bay of Bengal.

3 In the flood and drought years, most of notable predictive signals start appearing at approximately −4 days. However, there is a difference in the time of occurrence of similar predictive signals between the flood and drought years. Some predictive signals only appear in the flood years. Specifically, (a) NECC appears at approximately −8 days during the flood years but does not appear until approximately −4 days during the drought years. (b) LBAC appears at approximately −4 days in the flood years, but at −2 days in the drought years. (c) SCC-PSAC and the southeast and southwest WVFs appear at approximately −2 days in the flood years, but at −4 days in the drought years. The branch merging into the southwest WVFs from the waters near the Maldives appears at approximately −2 days in the drought years. (d) During the flood years, AAC and the southeast CEWVF are formed at approximately −4 days, but absent in the drought years. The results mentioned above can provide reference information for predicting LF precipitation intensity in South China.

6.2 | Discussion

We attempt to make a preliminary discussion on the reasons of the differences in LF water vapour transport between flood years and drought years from the following two aspects.

6.2.1 | The CEWVF and northwest water vapour wave trains

The southeast CEWVF existing in the flood years but absent in the drought years is taken as an example. In

the flood years, as shown in Figure 8, it comes from the northward WVF in the front of AAC located over the east of Australia. Cooperating with the PSAC, the northward WVF from the southwest Pacific Ocean is transported to South China. In the drought years, as shown in Figure 9, the AAC with a northwest–southeast direction extends from New Zealand to Western Australia and carries water vapour from the southwest Pacific Ocean to the Indian Ocean. At −2 days, it helps to form the southwest WVF branch near Maldives. Likewise, in the flood years, the southwest CEWVF is related to the Mascarene anticyclone. The specific mechanism of the southern hemisphere systems affecting the CEWVF will be further studied in the future. In addition, the LF water vapour wave trains in the northwest direction may be related to the energy dispersion of the LF Rossby waves. The preliminary studies have shown that the LF Rossby wave source from western Siberia causes circulation anomalies in eastern China through energy dispersion, and more Rossby wave energy reaches south China in the flood years than in the drought years (figure omitted), the results in detail will be given separately.

6.2.2 | SST anomaly

We all know that the inter-annual and LF variability of sea surface temperature (SST) may play an important role on generating atmospheric water vapour and its advection as one driving factor. For example, we found that El Niño-like (La Niña-like) SST anomaly took place in the pre-winter and pre-flood season over the Pacific for flood (drought) years (Figure 11). Some studies also disclosed that the intraseasonal SST anomaly is closely related to the intraseasonal rainfall anomaly in eastern China (Li and Luo, 2014). So the relationship among inter-annual and LF SST anomaly, water vapour transport and flood–drought events in the pre-flood season of South China is worthy of further research in more detail. In view of limited space, we will study this problem in another work carefully.

ACKNOWLEDGEMENTS

This research is supported jointly by National Key R&D Program of China (2018YFC1505602).

ORCID

Liping Li https://orcid.org/0000-0003-0976-8051

REFERENCES

Bao, M. (2008) Comparison of the effects of anomalous convective activities in the tropical Western Pacific on two persistent heavy rain events in South China. *Journal of Tropical Meteorology*, 24(1), 27–36.

Barlow, M., Wheeler, M., Luyon, B., et al. (2005) Modulation of daily precipitation over Southwest Asia by the Madden-Julian oscillation. *Monthly Weather Review*, 133(12), 3579–3594.

Bond, N.A. and Vecchi, G.A. (2003) The influence of the Madden-Julian oscillation on precipitation in Oregon and Washington. *Weather and Forecasting*, 18(4), 600–613.

Chan, J.C.L., Ai, W. and Xu, J.J. (2002) Mechanisms responsible for the maintenance of the 1998 South China Sea summer monsoon. *Journal of the Meteorological Society of Japan*, 80(5), 1103–1113.

Draxler, R.R. and Hess, G.D. (1998) An overview of HYSPLIT_4 modeling system for trajectories dispersion and deposition. *Australian Meteorological Magazine*, 47, 295–308.

Gao, S., Jian, M.Q. and Qiao, Y.T. (2010) Relationship between the 30–60 day oscillation of atmospheric heat source and the drought and flood events in June in the South China. *Journal of Tropical Meteorology*, 26(5), 555–562.

Hong, W., Ren, X.J. and Yang, X.Q. (2015) The influence of the low-frequency diabatic heating on the low-frequency circulation during the persistent severe rainfall period over South China. *Acta Meteorologica Sinica*, 73(2), 276–290.

Hu, Y.M., Zhai, P.M., Luo, X.L., et al. (2014) Large scale circulation and low frequency signal characteristics for the persistent extreme precipitation in the first rainy season over South China in 2013. *Acta Meteorologica Sinica*, 72(3), 465–477.

Huang, B., Thorne, P.W., et al. (2017) Extended Reconstructed Sea surface temperature version 5 (ERSSTv5), upgrades, validations, and intercomparisons. *Journal of Climate*, 30(20), 8179–8205.

Jeong, J.H., Kim, B.M., Ho, C.H., et al. (2008) Systematic variation in winter-time precipitation in East Asia by MJO-induced extratropical vertical motion. *Journal of Climate*, 21(4), 788–801.

Jones, C. (2000) Occurrence of extreme precipitation events in California and relationships with the Madden-Julian oscillation. *Journal of Climate*, 13(20), 3576–3587.

Ju, J.H., Sun, D. and Lv, J.M. (2007) The influence of the east Asian monsoon stream on the large-scale precipitation course in eastern China. *Chinese Journal of Atmospheric Sciences*, 31(6), 1129–1139.

Kistler, R., Kalnay, E., Collins, W., et al. (2001) The NCEP–NCAR 50-year reanalysis: monthly means CD-ROM and documentation. *Bulletin of the American Meteorological Society*, 82(2), 247–268.

Li, C.Y. (1993) *Low-Frequency Oscillation in the Atmosphere(Revised Edition)*. Beijing: *China Meteorological Press*, pp. 1–2.

Li, L.P. and Luo, T. (2014) Analysis on the relationship between the intraseasonal SST over the Northwest Pacific and summer intraseasonal rainfall in eastern China. *Transactions of Atmospheric Sciences*, 37(6), 715–722.

Li, W.K., He, J.H., Qi, L., et al. (2014a) The influence of the Madden-Julian oscillation on annually first rain season precipitation in South China and its possible mechanism. *Journal of Tropical Meteorology*, 30(5), 983–989.

Li, L.P., Xu, G.Y. and Liu, Y.J. (2014b) Influence of low-frequency moisture transportation on low-frequency precipitation

anomalies in the annually first rain season of South China in 2010. *Journal of Tropical Meteorology*, 30(3), 423–431.

Li, L.P., Yang, C.Y. and Kong, D.X. (2017) Low-frequency rainfall characteristics of the typical flood years in the annually first rainy season of South China and their relationships with low-frequency moisture transportation. *Journal of Tropical Meteorology*, 33(3), 299–312.

Lin, A.L., Liang, J.Y. and Gu, D.J. (2008) Review of impacts of tropical atmospheric intraseasonal oscillation on East Asia monsoon and mutiple time scales variation of tropical atmosphere intraseasonal oscillation. *Journal of Tropical Meteorology*, 24(1), 11–19.

Lin, A.L., Li, C.H., Gu, D.J., et al. (2013) Impact of tropical intraseasonal oscillation on the precipitation of Guangdong in Junes. *Journal of Tropical Meteorology*, 29(3), 353–363.

Madden, R.A. and Julian, P.R. (1971) Detection of a 40–50 day oscillation in the zonal wind in the tropical Pacific. *Journal of the Atmospheric Sciences*, 28(5), 702–708.

Madden, R.A. and Julian, P.R. (1972) Description of global scale circulation cells in the tropics with 40–50 day period. *Journal of the Atmospheric Sciences*, 29(6), 1109–1123.

Mao, J.Y. and Wu, G.X. (2005) Intraseasonal variability in the Yangtze-huaihe river rainfall and subtropical high during the 1991 Meiyu period. *Acta Meteorologica Sinica*, 63(5), 762–770.

Miao, R., Wen, M. and Zhang, R.H. (2017) Persistent precipitation anomalies and quasi-biweekly oscillation during the annually first rainy season over South China in 2010. *Journal of Tropical Meteorology*, 33(2), 155–166.

Murakami, M. (1984) Analysis of deep convective activity over the western Pacific and Southeast Asia. Part II: seasonal and intraseasonal variation during the northern summer[J]. *Journal of the Meteorological Society of Japan*, 62(1), 88–108.

Pohl, B., Richard, Y. and Fauchereau, N. (2007) Influence of the Madden-Julian oscillation on southern African summer rainfall. *Journal of Climate*, 20(16), 4227–4242.

Shi, X.L. and Ding, Y.H. (2000) A study on extensive heavy rain processes in South China and the summer monsoon activity in 1994. *Acta Meteorologica Sinica*, 58(6), 666–678.

Tang, T.Y., Wu, C.S., Wang, A.Y., et al. (2007) An observational study of interaseasonal variations over Guangdong province China during the rainy season of 1999. *Journal of Tropical Meteorology*, 23(6), 683–689.

Tao, S.Y. and Wei, J. (2007) Correlation between monsoon surge and heavy rainfall causing flash-flood in southern China in summer. *Meteorological Monthly*, 33(3), 10–18.

Wei, F.Y. (2009) *Modern Climate Statistical Diagnosis and Prediction Techniques*. Beijing: *China Meteorological Press*.

Wheeler, M.C., Hendon, H.H., Cleland, S., et al. (2009) Impacts of the Madden-Julian oscillation on Australian rainfall and circulation. *Journal of Climate*, 22(6), 1482–1498.

Wu, H.B. and Wu, L. (2005) *Diagnosis and Prediction Method of Climate Variability*. Beijing: *China Meteorological Press*, pp. 208–225.

Xie, Y.B., Chen, S.L., Zhang, Y.L., et al. (1963) A preliminarily statistic and synoptic study about the basic flows over southeastern Asia and the initiation of typhoons. *Acta Meteorologica Sinica*, 33(2), 206–217.

Xin, F., Xiao, Z.N. and Li, Z.C. (2007) Relation between flood season precipitation anomalies in South China and east Asian atmospheric low frequency oscillation in 1997. *Meteorological Monthly*, 33(12), 23–30.

Xu, G.Y., Yang, H., Wang, X.F., et al. (2018) Study on the low-frequency features of precipitation in serious flood and drought pre-flood seasons over South China and its relationship with cold air. *Journal of the Meteorological Sciences*, 38 (2), 167–176.

Zhang, L.N., Wang, B.Z. and Zeng, Q.C. (2009) Impact of the Madden-Julian oscillation on summer rainfall in Southeast China. *Journal of Climate*, 22(2), 201–216.

Zhang, L.N., Lin, P.F., Xiong, Z., et al. (2011) Impact of the Madden-Julian oscillation on pre-flood season precipitation in South China. *Chinese Journal of Atmospheric Sciences*, 35(3), 560–570.

Zhang, Y.H., Zhou, B. and Zhang, Y.C. (2012) Abnormality of general circulation with LFO during the torrential rainstorms over southern China in 2010. *Meteorological Monthly*, 38(11), 1367–1377.

How to cite this article: Li L, Ma C, Yang C. Study on the differences in water vapour characteristics and predictive signals of low-frequency precipitation in the pre-flood season of South China between flood and drought years. *Int J Climatol*. 2020;1–16. https://doi.org/10.1002/joc.6600

APPENDIX A.

LEAD–LAG CORRELATION

An introduction to the idea of calculating the lead–lag correlation coefficient between low-frequency water vapour flux and precipitation is given as follows.

First, the regional average LF precipitation time series is calculated for each flood (drought) year. Because there are eight (seven) typical flood (drought) years, a $8 \times 91 = 728$ ($7 \times 91 = 637$)-day LF precipitation sample connected in sequence from April 1 to June 30 is obtained. Similarly, there is a $8 \times 91 = 728$ ($7 \times 91 = 637$)-day sample for LF water vapour flux field in the flood (drought) years. Table 2 gives the specific dates of LF water vapour flux field time series every year for lead–lag correlation calculation of different days ahead. For instance, Figure 8 at −2 days is gotten by calculating the Pearson correlation coefficients between the meridional and zonal LF water vapour flux field series from March 30 to June 28 and the regional average LF precipitation sequence from April 1 to June 30 connected in sequence for eight typical flood years. The correlation coefficients are tested by *t*-test method. As long as one of the meridional and zonal correlation coefficients is significant, the corresponding vector composed of them is drawn.

TABLE 2 The specific dates of LF water vapour flux field time series every year for lead–lag correlation of different days ahead

Lead days	Dates
−8 days	March 24 to June 22
−6 days	March 26 to June 24
−4 days	March 28 to June 26
−2 days	March 30 to June 28
0 days	April 1 to June 30

APPENDIX B.

HYSPLIT DISPERSION TRAJECTORY CALCULATION METHOD

The advection of a particle or puff is computed from the average of the three dimensional velocity vectors for the initial-position $P(t)$ and the first-guess position $P'(t + \Delta t)$. The velocity vectors are linearly interpolated in both space and time. The first guess position is,

$$P'(t+\Delta t)=P(t)+V(P,t)\Delta t \quad \text{(A1)}$$

and the final position is,

$$P(t+\Delta t)=P(t)+0.5[V(P,t)+V(P',t+\Delta t)]\Delta t \quad \text{(A2)}$$

The maximum transport velocity $U_{\max}$ is determined from the maximum particle/puff transport speed during the previous hour. The integration time step (Δt) can vary from 1 min to 1 hr during the simulation. The advection distance per time-step should be less than the grid spacing, which meets the following formula.

$$U_{\max}\left(\text{grid-units}\,\text{min}^{-1}\right)\Delta t(\text{min})<0.75(\text{grid-units}) \quad \text{(A3)}$$